# Ferrous iron partitioning between magnesium silicate perovskite and ferropericlase and the composition of perovskite in the Earth's lower mantle

Yoichi Nakajima,[1] Daniel J. Frost,[1] and David C. Rubie[1]

Received 10 January 2012; revised 25 May 2012; accepted 15 June 2012; published 2 August 2012.

[1] We have investigated the exchange of Fe and Mg between magnesium silicate perovskite (Mg-Pv) and ferropericlase (Fp) at 25 GPa and 2400 to 2600 K using a Kawai-type multianvil apparatus. Each experiment was performed with coexisting metallic Fe, which buffered the oxygen fugacity at the lowest possible level. As the system was Al-free the presence of metallic Fe ensures low ferric iron ($Fe^{3+}$) contents in all phases. The results are used to extract thermodynamic data to describe $Fe^{2+}$-Mg partitioning. A thermodynamic assessment and modeling of the available high-pressure partitioning data indicates that the influence of a Fe-spin transition in Fp on Fe-Mg partitioning may be more subtle than previously proposed. Furthermore, we demonstrate that a comparison between perovskite $Fe^{2+}$ contents predicted by the thermodynamic model and previously reported perovskite analyses can be used to estimate Mg-Pv $Fe^{3+}$ concentrations of both Al-bearing and Al-free phases in the previous studies. These estimates show that the $Fe^{3+}$ content of Al-free Mg-Pv depends strongly on oxygen fugacity, and varies accordingly with the capsule materials used in experiments. The relationship between $Fe^{3+}$ and Al concentrations in Al-bearing Mg-Pv indicates that the substitution mechanism of $Fe^{3+}$ and Al changes with Al content. Chemical heterogeneities in the lower mantle will result in the formation of Mg-Pv with quite different Al and bulk Fe concentrations, which will cause important differences in $Fe^{3+}$ and oxygen vacancy concentrations in Mg-Pv.

**Citation:** Nakajima, Y., D. J. Frost, and D. C. Rubie (2012), Ferrous iron partitioning between magnesium silicate perovskite and ferropericlase and the composition of perovskite in the Earth's lower mantle, *J. Geophys. Res.*, *117*, B08201, doi:10.1029/2012JB009151.

## 1. Introduction

[2] $(Mg,Fe)SiO_3$ perovskite (Mg-Pv) and (Mg,Fe)O ferropericlase (Fp) comprise more than 90 volume % of the Earth's lower mantle [e.g., *Irifune*, 1994]. Knowledge of the chemical and physical properties of these phases is, therefore, essential for understanding the structure and dynamics of the lower mantle. The partitioning of Fe between the dominant lower mantle phases has been intensively studied because the iron contents of the respective phases will influence lower mantle transport properties such as rheology, elasticity, and electrical and thermal conductivities [e.g., *Mao et al.*, 1997]. The sharpness, i.e., pressure/depth interval, of the post-spinel transition from $(Mg,Fe)_2SiO_4$ spinel to Mg-Pv and Fp, which is considered to cause the 660 km seismic discontinuity, will depend mainly on the partitioning of Fe-Mg between the transforming phases [*Ito and Takahashi*, 1989]. Seismic studies argue that this is a remarkably sharp phase transformation occurring over a depth interval corresponding to only a few tenths of a gigapascal (GPa) [e.g., *Benz and Vidale*, 1993]. In addition, changes in the Fe spin state have also been considered to influence Fe-Mg partitioning [e.g., *Badro et al.*, 2003; *Lin et al.*, 2005; *Irifune et al.*, 2010]. In a reciprocal fashion, the onset pressure of the spin transition will also be influenced by the Fe content of the phase [*Fei et al.*, 2007].

[3] The partitioning of Fe-Mg between Mg-Pv and Fp can be described using the exchange, or distribution coefficient, $K_D$:

$$K_D = \left(X^{Pv}_{FeSiO_3} \Big/ X^{Pv}_{MgSiO_3}\right) \Big/ \left(X^{Fp}_{FeO} \Big/ X^{Fp}_{MgO}\right), \qquad (1)$$

where $X^a_i$ is the mole fraction of component $i$ in phase $a$. Ideally $K_D$ describes $Fe^{2+}$-Mg partitioning where, for example, $X^{Pv}_{FeSiO_3}$ is equal to the molar ratio $Fe^{2+}/(Fe^{2+} + Mg)$. However, in most studies $Fe^{3+}/\Sigma Fe$ ($\Sigma Fe = Fe^{2+} + Fe^{3+}$) ratios of phases have not been determined and an apparent $K_D$ or $K_D(app)$ is actually measured where $X^{Pv}_{FeSiO_3}$ is, in reality, the molar ratio $(Fe^{2+} + Fe^{3+})/(Fe^{2+} + Fe^{3+} + Mg)$.

[1]Bayerisches Geoinstitut, Universität Bayreuth, Bayreuth, Germany.

Corresponding author: Y. Nakajima, Bayerisches Geoinstitut, Universität Bayreuth, D-95440 Bayreuth, Germany. (yoichi.nakajima@uni-bayreuth.de)


0148-0227/12/2012JB009151

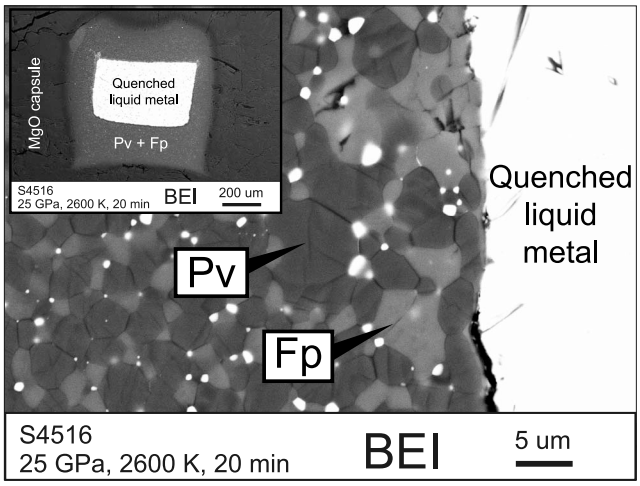


**Figure 1.** Backscattered electron image (BEI) of a recovered sample that consists of quenched liquid metal coexisting with Mg-perovskite (Pv) and ferropericlase (Fp). The inset shows a low-magnification image of the entire sample contained in an MgO capsule.

[4] A number of experiments employing both natural mantle compositions and compositions in the simple MgO-FeO-$SiO_2$ system have been performed using the multianvil apparatus and diamond anvil cells to investigate temperature, pressure, and composition effects on $K_D$. There are many discrepancies between experimental studies, even in simplified systems, and particularly between studies performed at pressures higher than 25 GPa in the laser-heated diamond anvil cell [*Auzende et al.*, 2008; *Sakai et al.*, 2009; *Sinmyo et al.*, 2008]. A number of possible explanations exist for experimental and analytical discrepancies such as sluggish kinetics of chemical equilibration [*Katsura and Ito*, 1996; *Frost and Langenhorst*, 2002] and heterogeneity in the chemical composition and temperature of the samples [*Sinmyo et al.*, 2008]. The valence state of iron in Mg-Pv and Fp will also have a strong effect on $K_D$, or at least on apparent $K_D$ values derived from electron microprobe and transmitting electron microscopy analyses because the definition of $K_D$ describes only ferrous iron ($Fe^{2+}$) exchange.

[5] The ratio of ferric to ferrous iron in both minerals depends to some extent on oxygen fugacity but for Mg-Pv the Al concentration has by far the most dramatic influence [*Frost and Langenhorst*, 2002; *McCammon et al.*, 2004]. Ferric iron is favorably partitioned into Mg-Pv, particularly in Al-bearing systems, whereas ferrous iron is preferentially partitioned into Fp. This opposing behavior complicates partitioning determinations as it requires ferrous and ferric Fe to be distinguished in the recovered samples and, for a rigorous description, requires either control or measurement of the experimental oxygen fugacity. Due to these complications some uncertainties in the effects of $fo_2$ and temperature still exist for Fe partitioning behavior between Mg-Pv and Fp, even for Al-free systems at pressures attainable by the large-volume multianvil apparatus. More importantly, partitioning trends determined at relatively well-constrained conditions in multianvil experiments are crucial for evaluating results obtained at higher pressures in the diamond anvil cell [e.g., *Auzende et al.*, 2008; *Sinmyo et al.*, 2008] and for determining the thermodynamic parameters that are required to extrapolate partitioning behavior to higher pressures and temperatures.

[6] In this study we have examined the exchange coefficient of Fe between Mg-Pv and Fp at low-oxygen fugacity imposed by the coexistence of metallic Fe. These conditions ensure low levels of ferric Fe in each phase over the range of compositions investigated and thus allow $Fe^{2+}$-Mg partitioning to be characterized. Experiments were performed at high temperatures of 2400–2600 K, i.e., close to the silicate solidus, to alleviate kinetic problems observed at lower temperatures in metallic Fe-bearing systems [*Frost and Langenhorst*, 2002].

## 2. Experimental and Analytical Procedure

[7] High-pressure experiments were carried out at a pressure of 25 GPa using a Kawai-type multianvil apparatus at the Bayerisches Geoinstitut. In each experiment, a 10-mm MgO octahedral pressure medium was compressed by tungsten-carbide cubes with 4 mm truncated edge lengths (10/4 assembly). A cylindrical $LaCrO_3$ heater was employed and the temperature was measured using a W3%Re-W25% Re thermocouple. Further experimental details are described by *Frost and Langenhorst* [2002].

[8] Different compositions of $(Mg_{1-x},Fe_x)_2SiO_4$ olivine (Fo#70, 90, 95, where Fo# = $(1-x) \times 100$,) were prepared as starting compositions. Olivine Fo70 and Fo95 samples were synthesized from regent grade oxide mixtures using a $CO$-$CO_2$ gas mixing furnace at 1200°C and log $fo_2 = -11.0$. Natural powdered San Carlos olivine was employed for the Fo90 composition. Olivine powder was packed together with a piece of 0.5 mm diameter Fe-wire into an MgO single crystal capsule. The samples were compressed to 25 GPa and then annealed at temperatures between 2400 and 2600 K for 10–60 min. The temperature uncertainties are estimated to be less than $\pm$ 100 K based on the reproducibility of the temperature-power relationship. The recovered samples were examined by Raman spectroscopy and scanning electron microscope with an electron backscattered diffractometer. Quantitative chemical analyses were performed using an electron microprobe with a wavelength dispersive x-ray spectrometer. Operating conditions were 15 kV and 10 nA with a focused beam. The measurement time for each element was 20–30 s. $Mg_2SiO_4$ forsterite and metallic Fe were used as internal standards.

## 3. Results

### 3.1. Fe-Mg Distribution Coefficients

[9] A backscattered electron image of a typical run product is shown in Figure 1. The recovered samples consisted of Mg-Pv and Fp together with metallic Fe, and no other phases were observed. From textural observations, the metallic iron melted at temperatures above 2350 K. The grain sizes of Mg-Pv and Fp near the liquid metal are large (>5 $\mu$m) relative to those found further from the metal, implying that liquid metal may act as a catalyst for grain growth. This catalytic effect also appears to promote chemical equilibrium (or at least chemical phase homogeneity) between coexisting Mg-Pv and Fp phases [*Katsura and Ito*, 1996]. The chemical compositions of Mg-Pv and Fp were obtained from grains

**Table 1.** Experimental Conditions and Compositions of Perovskite and Ferropericlase[a]

| Run | Starting Materials | $T$ (K) | Duration (min) | $X_{Fe}$[b] | | $K_D$[c] | $\Delta$IW[d] |
|---|---|---|---|---|---|---|---|
| | | | | Pv | Fp | | |
| S4797 | Fo70 | 2450 | 10 | 0.110(3) | 0.323(4) | 0.26(1) | −0.64(3) |
| S4882 | Fo70 | 2500 | 40 | 0.161(15) | 0.487(24) | 0.20(3) | −0.43(7) |
| S4434 | Fo90 | 2430 | 60 | 0.071(4) | 0.235(9) | 0.25(2) | −0.88(8) |
| S4527 | Fo90 | 2500 | 10 | 0.070(4) | 0.191(2) | 0.32(2) | −1.02(3) |
| S4796 | Fo90 | 2550 | 20 | 0.064(3) | 0.188(2) | 0.29(2) | −1.03(4) |
| S4441 | Fo90 | 2573 | 30 | 0.073(6) | 0.210(3) | 0.30(3) | −0.94(3) |
| S4510 | Fo95 | 2400 | 10 | 0.061(2) | 0.177(17) | 0.30(4) | −1.07(20) |
| S4545 | Fo95 | 2590 | 30 | 0.047(2) | 0.119(2) | 0.37(2) | −1.38(3) |
| S4516 | Fo95 | 2600 | 20 | 0.058(3) | 0.147(4) | 0.35(2) | −1.19(6) |
| S4555 | Fo95 | 2600 | 30 | 0.044(3) | 0.122(3) | 0.33(2) | −1.35(7) |

[a]Numbers between parentheses are one standard deviation.
[b]Fe/(Fe + Mg)
[c]$K_D = (X_{Fe}^{Pv}/X_{Mg}^{Pv})/(X_{Fe}^{Fp}/X_{Mg}^{Fp})$.
[d]Oxygen fugacity relative to iron-wüstite buffer.

adjacent to liquid metal. Although localized chemical compositional changes occurred as a result of reaction with the metal, the composition of each phase in each experiment was relatively constant in the proximity of the liquid metal, within the uncertainties listed in Table 1.

[10] Compositional data and distribution coefficients are summarized together with the experimental conditions in Table 1. No significant change in $K_D$ was observed between experiments performed at similar conditions for annealing times of 10 and 60 min, implying that for temperatures in the range 2400–2600 K and in the presence of liquid Fe metal, chemical equilibrium is achieved within 10 min. The oxygen fugacity was calculated from Fe and FeO concentrations in metal and ferropericlase respectively [*Mann et al.*, 2009] and log $fo_2$ values are reported relative to the iron-wüstite oxygen buffer ($\Delta$IW). The oxygen fugacity range in the experiments is between $\Delta$IW-0.4 and $\Delta$IW-1.4, with the lowest oxygen fugacities corresponding to the samples with the lowest bulk FeO contents.

[11] The Mg-Pv and Fp distribution coefficients for Fe-Mg partitioning are plotted in Figure 2 as a function of the mole fraction of FeO in Fp. Iron preferentially partitions into Fp but higher temperatures result in higher values of $K_D$, i.e., a decrease in the Fe preference for Fp. This trend is even more apparent when the results of *Frost and Langenhorst* [2002] and *McCammon et al.* [2004] are considered, which were obtained at temperatures <2000 K (Figure 2).

[12] Mössbauer spectroscopy measurements [*Frost et al.*, 2001; *McCammon et al.*, 2004] indicate that $Fe^{3+}$ concentrations in ferropericlase coexisting with metallic iron at high pressures, >18 GPa, are negligible for Fe/(Fe + Mg) ratios <0.5 (Figure 3). It should be noted, however, that although the Fp $Fe^{3+}$ contents are negligible for Fe/(Fe + Mg) ratios obtained in the current study, the $Fe^{3+}/\Sigma Fe$ ratio of Fp will be small but significant (2–5%) for Fe/(Fe + Mg) ratios >0.8 [*McCammon*, 1992; *Frost et al.*, 2001].

[13] For Mg-Pv in the Al-free system, the dominant influences on the $Fe^{3+}$ content are the total Fe concentration and oxygen fugacity [*McCammon et al.*, 1997, 2004]. For Al-free $(Mg,Fe)SiO_3$ perovskite coexisting with metallic Fe with Fe/(Fe + Mg) ratios <0.2, $Fe^{3+}/\Sigma Fe$ values in the range 0.07 to 0.1 have been reported [*Lauterbach et al.*, 2000; *McCammon et al.*, 1997]. In the present study the Fe/(Mg + Fe) ratios of Mg-Pv lie in the range 0.04–0.15 and the $Fe^{3+}$ concentrations will therefore be at a similar level to the analysis errors (Table 1). As a result of buffering $Fe^{3+}$ levels at the lowest practical level we can assume that the partitioning results dominantly describe $Fe^{2+}$-Mg partitioning with a negligible effect of $Fe^{3+}$ such that the apparent $K_D$ or $K_D(app) \approx K_D$.

### 3.2. Thermodynamics of Fe-Mg Partitioning Between Perovskite and Ferropericlase

[14] The $Fe^{2+}$ and Mg exchange equilibrium between Mg-Pv and Fp is

$$MgSiO_3^{Pv} + Fe^{2+}O^{Fp} \leftrightarrow Fe^{2+}SiO_3^{Pv} + MgO^{Fp}. \quad (2)$$

The distribution coefficient $K_D$ is then defined as in equation (1). At equilibrium $K_D$ can be described by the expression:

$$RT\ln K_D = -\Delta G_{P,T}^0 - W_{FeMg}^{Pv}\left(1 - 2X_{FeSiO3}^{Pv}\right) + W_{FeMg}^{Fp}\left(1 - 2X_{FeO}^{Fp}\right), \quad (3)$$

where $R$ is the gas constant, $\Delta G_{P,T}^0$ is the standard state Gibbs free energy change for the pure end-member equilibrium at the pressure and temperature of interest and $W_{FeMg}^{Pv}$ and $W_{FeMg}^{Fp}$ are symmetric interaction parameters (Margules parameters) for Mg-Pv and Fp that account for the non-ideality of Fe-Mg mixing in each solid solution. The standard state Gibbs free energy change for equilibrium (2) can be simply described by

$$\Delta G_{P,T}^0 = \Delta H^0 + P\Delta V^0 - T\Delta S^0, \quad (4)$$

where $\Delta H^0$, $\Delta V^0$, and $\Delta S^0$ are changes in enthalpy, volume, and entropy, respectively. Equations (3) and (4) can be fit to the experimental data and to the results of *Frost and Langenhorst* [2002]. However, as the two interaction parameters are highly correlated it is more practical to fix one of these parameters using results of previous studies. The Margules parameter $W_{FeMg}^{Fp}$ for ferropericlase has been well

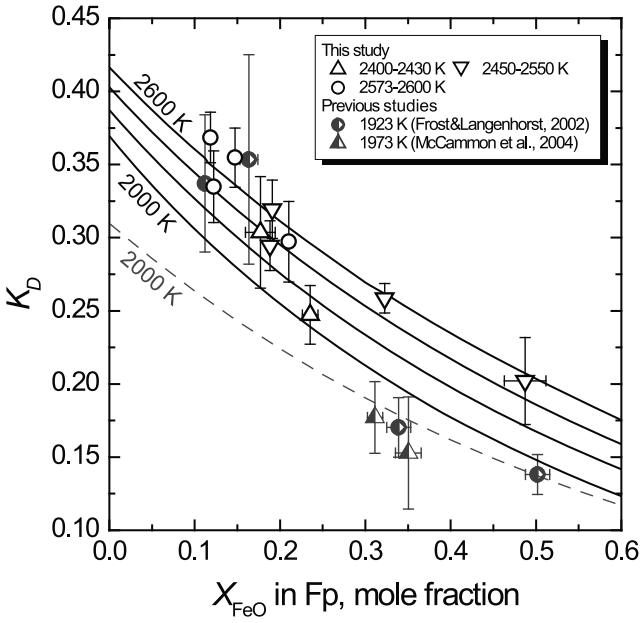


**Figure 2.** Experimental results of Fe-Mg partitioning between Pv and Fp plotted as $K_D$ against $X_{FeO}$ in Fp. Results from the previous studies of *Frost and Langenhorst* [2002] and *McCammon et al.* [2004] are also shown. The solid lines show isothermal $K_D$ values (200 K intervals) that result from fitting equation (3) to the data. The broken line shows $K_D$ calculated from the thermodynamic parameters proposed by *McCammon et al.* [2004].

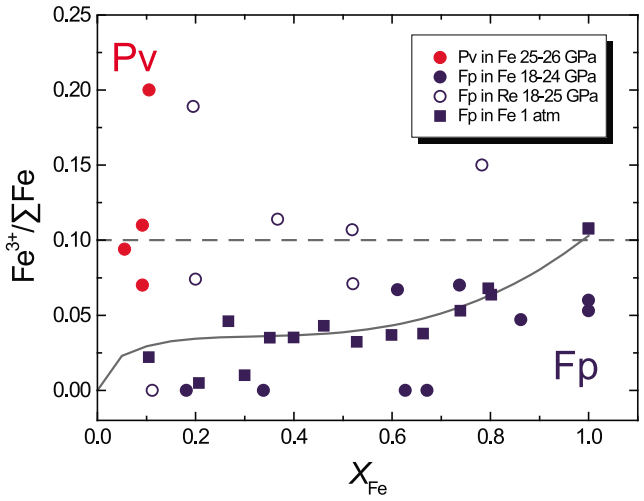


**Figure 3.** Ferric iron contents of perovskite and ferropericlase. Values of ferric iron relative to total iron content ($Fe^{3+}/\Sigma Fe$) in perovskite (Pv – red symbols) and ferropericlase (Fp – blue symbols) are plotted as a function of $X_{Fe}$. Perovskite data are from *Lauterbach et al.* [2000] and *McCammon et al.* [1997]. Data for ferropericlase coexisting with metallic Fe were obtained at 1 bar [*Katsura and Kimura*, 1965; *O'Neill et al.*, 2003; *Srečec et al.*, 1987] and at 18–24 GPa [*Frost et al.*, 2001]. Data for ferropericlase contained in Re capsules are from *Frost et al.* [2001] and *Frost and Langenhorst* [2002]. Solid and broken lines show calculated $Fe^{3+}/\Sigma Fe$ ratios of Fp coexisting with metallic Fe [*O'Neill et al.*, 2003] and Re (this study), respectively.

studied over a wide pressure, temperature and compositional range [*Frost*, 2003] and $W^{Fp}_{FeMg}$ = 14 kJ/mol at 25 GPa is taken from this previous work. By fitting to the 25 GPa results the following terms are derived: $\Delta H^0 + P\Delta V^0$ = 27.2 ± 6.6 kJ/mol, $\Delta S^0 = -4.0 \pm 1.9$ J/mol $K^{-1}$, and $W^{Pv}_{FeMg} = -4.9 \pm 7.6$ kJ/mol. Because the compositional range of $X^{Pv}_{FeSiO_3}$ = 0.04–0.15 covered by this study is small, the uncertainty of $W^{Pv}_{FeMg}$ is relatively large and fixing $W^{Pv}_{FeMg}$ to be 0 kJ/mol is equally justified. The expression for $\Delta G^0_{P,T}$ then becomes $\Delta H^0 + P\Delta V^0$ = 24.1 ± 4.4 kJ/mol and $\Delta S^0 = -3.5 \pm 1.7$ J/mol $K^{-1}$. The fitted curves calculated using obtained parameters with $W^{Pv}_{FeMg} = -4.9$ kJ/mol are shown in Figure 2.

## 4. Discussion

### 4.1. Comparison With Previous Thermodynamic Models and Calculating the Depth Interval of the 660 km Seismic Discontinuity

[15] Using the present experimental data and fixing interaction parameters for Mg-Pv and Fp as given in the last section, we have calculated the standard state Gibbs free energy change $\Delta G^0_{P,T}$ for equilibrium (2) at 25 GPa from equation (3) (Figure 4). The uncertainties in $\Delta G^0_{P,T}$ were propagated mainly from the uncertainty in the determination of $W^{Pv}_{FeMg}$. The effect of temperature uncertainty on the $\Delta G^0_{P,T}$ calculation is negligible, even when taking the maximum uncertainty (100 K) of the present temperature measurements into

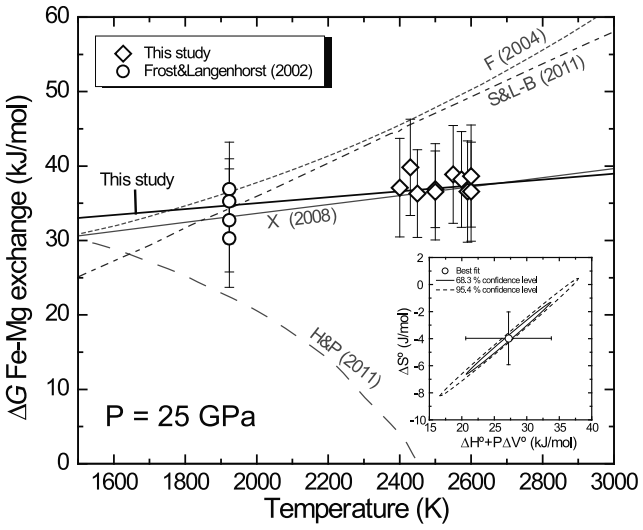


**Figure 4.** The standard state Gibbs free energy change ($\Delta G^0_{P,T}$) of the $Fe^{2+}$-Mg exchange reaction between perovskite and ferropericlase at 25 GPa as a function of temperature. The Gibbs free energies were obtained from isothermal fits of equation (3) to the present results and those of previous studies [*Frost and Langenhorst*, 2002]. The black line shows the best fit to these data. The labeled gray lines are from thermodynamic models by *Fabrichnaya et al.* [2004]: F (2004), *Holland and Powell* [2011]: H&P (2011), *Stixrude and Lithgow-Bertelloni* [2011]: S&L-B (2011), and *Xu et al.* [2008]: X (2008). The inset shows the confidence ellipsoid from the determination of the entropy change ($\Delta S^0$) and enthalpy and volume change ($\Delta H^0 + P\Delta V^0$).

**Table 2.** Properties of End-Member Components for the Helmholtz Free Energy Calculation[a]

| | $F_0$ (kJ/mol) | $V_0$ (cc/mol) | $K_0$ (GPa) | $K_0'$ | $\theta_0$ (K) | $\gamma_0$ | $q_0$ | References |
|---|---|---|---|---|---|---|---|---|
| $MgSiO_3$_Pv | −1368 | 24.45 | 251 | 4.1 | 905 | 1.57 | 1.1 | *Xu et al.* [2008] |
| $FeSiO_3$_Pv | −1018 | 25.40 | 272 | 4.1 | 765 | 1.44 | 1.4 | *Xu et al.* [2008] |
| $FeSiO_3$_Pv[b] | −1023 | 25.34 | 272 | 4.1 | 765 | 1.44 | 1.4 | *Xu et al.* [2008], *Tange et al.* [2009], this study |
| MgO | −570 | 11.24 | 161 | 3.9 | 772 | 1.48 | 1.6 | *Xu et al.* [2008] |
| FeO | −244 | 12.26 | 179 | 4.9 | 454 | 1.54 | 1.6 | *Xu et al.* [2008] |
| FeO[b] | −244 | 12.26 | 149.4 | 3.6 | 417 | 1.41 | 0.5 | *Xu et al.* [2008], *Fischer et al.* [2011] |

[a]Helmholtz free energy, $F_0$, volume, $V_0$, bulk modulus, $K_0$, pressure derivative of the bulk modulus, $K_0'$, Debye temperature, $\theta_0$, Grüneisen parameter, $\gamma_0$, logarithmic volume derivative of the Grüneisen parameter, $q_0$, at ambient conditions.
[b]Zero pressure volume of $FeSiO_3$-Pv and thermoelastic parameters of FeO are taken from recent experimental studies instead of the original values used in *Xu et al.* [2008].

account. The $\Delta G^0_{P,T}$ values, calculated by also employing the results of previous experiments [*Frost and Langenhorst*, 2002], indicate a weak dependence on temperature, corresponding to an entropy change ($\Delta S^0$) of −4.0 J/mol K. The insert of Figure 4 shows confidence ellipsoids for the fitted $\Delta S^0$ and $\Delta H^0 + P\Delta V^0$ values, indicating that the uncertainties on each term are highly correlated.

[16] This determination of $\Delta G^0_{P,T}$ provides the only rigorous approach for approximating the Gibbs free energy for the $FeSiO_3$ perovskite end-member because all other end-members in equilibrium (2) can be estimated independently. Similarly these results can be used to test predictions of existing thermodynamic databases for the calculation of $\Delta G^0_{P,T}$ as shown in Figure 4. Results show that several previous studies provide poor estimates for $\Delta G^0_{P,T}$ particularly at high temperature. Differences between the experimental results and thermodynamic calculations of *Fabrichnaya et al.* [2004], *Holland and Powell* [2011], and *Stixrude and Lithgow-Bertelloni* [2011] become large at temperatures >2000 K, but excellent agreement is found with the study of *Xu et al.* [2008]. Since lower mantle temperatures lie in the range 1900–2700 K [e.g., *Stacey and Davis*, 2004], reliable thermodynamic data at high temperatures are critical for modeling the lower mantle.

[17] The ability to accurately determine $\Delta G^0_{P,T}$ for equilibrium (2) is essential for calculating the pressure or depth interval of the $(Mg_{0.9},Fe_{0.1})_2SiO_4$ ringwoodite to Mg-Pv + Fp transformation, which is considered to cause the 660 km seismic discontinuity. As the transformation is divariant and Fe and Mg partition differently between the three phases, it occurs over a specific pressure interval within which all three phases coexist. Seismology can provide a qualitative estimate for the depth interval of the corresponding jump in seismic velocities in the Earth. Using data consistent with Figure 4 and ringwoodite Fe-Mg mixing parameters from *Frost et al.* [2001] this pressure interval can be calculated to be 0.025 GPa at 1873 K, which corresponds to a depth interval in the Earth of less than 1 km. Such a narrow interval would be impossible to determine through phase equilibrium experiments. Although the presence of Al in the Earth may serve to broaden this transition to some extent, experimental studies have shown relatively small Al concentrations in Mg-Pv at the pressure of the transformation [*Hirose*, 2002]. Such a sharp depth interval is in excellent agreement with seismic observations [e.g., *Benz and Vidale*, 1993] that indicate a sharp 660 km discontinuity capable of reflecting short period seismic waves.

### 4.2. Effect of Pressure on Fe-Mg Partitioning

[18] The effect of pressure on $K_D$ has been intensely investigated through diamond anvil cell (DAC) experiments. There are, however, significant inconsistencies between some studies, and even between those performed using the same starting material (e.g., natural San Carlos olivine) and under similar experimental conditions [*Auzende et al.*, 2008; *Kobayashi et al.*, 2005; *Sakai et al.*, 2009; *Sinmyo et al.*, 2008]. Using the data from this study, the temperature and compositional effects on Fe-Mg partitioning can be described and by making some assumptions about the volume change of equilibrium (2), an assessment of the likely effect of pressure can be made. This is important because without some basic understanding of the plausible magnitude of the pressure dependence, anomalous behavior that might arise from changes in the Fe-spin state in either phase cannot be recognized.

[19] Two methods are used here to assess the likely pressure dependence of Fe-Mg partitioning. The first uses thermodynamic data on Mg-Pv and Fp, extrapolated using an equation of state model, while the second uses the high-pressure data themselves to assess the volume change implied by each experimental date point.

[20] For the first method of extrapolation, independent estimates of the volumetric and equation of state (EoS) properties of the components in equilibrium (2) are used in the EoS model of *Xu et al.* [2008] to calculate values of $K_D$ at high pressure. The calculation is made for a $(Mg_{0.9},Fe_{0.1})_2SiO_4$ composition at 2000 K, i.e., similar to most DAC samples [*Auzende et al.*, 2008; *Sakai et al.*, 2009; *Sinmyo et al.*, 2008]. The thermodynamic parameters used in the calculation are given in Table 2. $K_D$ values were calculated using the model of Xu et al. to determine $\Delta G^0_{P,T}$ for equilibrium (2) at high $P$-$T$ conditions and using the Margules parameters $W^{Pv}_{FeMg}$ and $W^{Fp}_{FeMg}$ obtained in this study (see section 3.2). The effect of pressure on $W^{Fp}_{FeMg}$was taken from *Frost* [2003], whereas that on $W^{Pv}_{FeMg}$ was considered to be zero in the absence of evidence to the contrary. As can be seen in Figure 5, $K_D$ values predicted using this approach are considerably higher than the results of most experimental studies. The differences between the calculated $K_D$ and experimental data become significant with increasing pressure and it is clear that the EoS model of Xu et al. does not reproduce the volume change of equilibrium (2). This inconsistency might be alleviated through the selection of different EoS parameters for the various components with terms for $FeSiO_3$-Pv and FeO being the most uncertain.

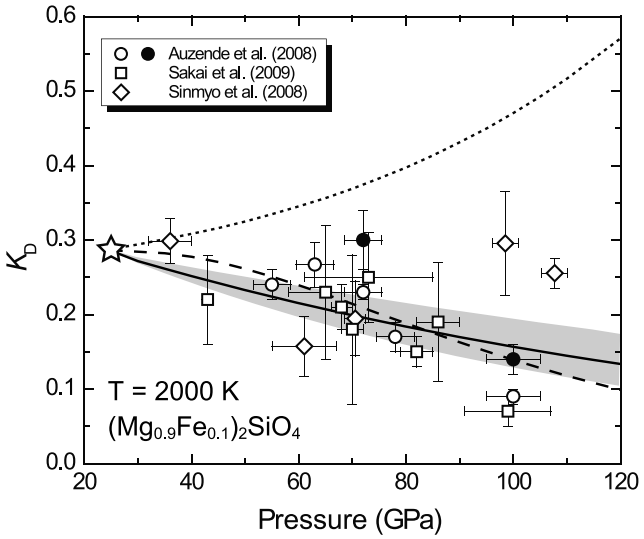


**Figure 5.** The effect of pressure on Fe-Mg partitioning ($K_D$). The solid line shows the $K_D$ for a $(Mg_{0.9}, Fe_{0.1})_2SiO_4$ composition at 2000 K calculated from equation (6) by assuming the average volume change ($0.20 \pm 0.04$ cm$^3$/mol) for the ion exchange equilibrium determined by considering all available DAC experimental data (see Figure 6 and text for details). The gray region shows the uncertainty on this $K_D$ estimate propagated from the resultant volume change uncertainty. The dotted line is calculated from the thermodynamic model of *Xu et al.* [2008]. The dashed line is also calculated using the same model of *Xu et al.* [2008] but with the EoS data for FeO replaced by those from the recent experimental study of *Fischer et al.* [2011] and the ambient volume of $FeSiO_3$ replaced by that of *Tange et al.* [2009]. These $K_D$ calculations are compared with previous DAC experiments performed with similar starting compositions and at temperature conditions of 2000–2450 [*Auzende et al.*, 2008], 1860–2120 K [*Sakai et al.*, 2009] and 1760–2170 K [*Sinmyo et al.*, 2008]. Open and filled symbols show transmission electron microscopy (TEM) and secondary ion mass spectroscopy (SIMS) measurements, respectively.

The FeO EoS employed by *Xu et al.* [2008], for example, predicts relatively large volumes at high pressure, compared to the recent experimental study of *Fischer et al.* [2011]. We found that modification of the zero-pressure volume of $FeSiO_3$-Pv and the EoS of FeO based on the recent studies of *Tange et al.* [2009] and *Fischer et al.* [2011], respectively, lead to calculated $K_D$ values which are in much better agreement with the experimental DAC partition data. The $K_D$ calculated using these modified EoS parameters (Table 2) is shown by the dashed line in Figure 5.

[21] The second approach is to use equations (3) and (4) to calculate $K_D$, where the pressure effect is simply described by a constant volume change $\Delta V^0$of reaction (2) and the remaining terms are determined using the results from this study. $\Delta V^0$ can be evaluated using each experimental data point from the previous DAC experiments performed over the entire lower-mantle pressure range [*Auzende et al.*, 2008; *Kobayashi et al.*, 2005; *Sakai et al.*, 2009; *Sinmyo et al.*, 2008]. From the $K_D(P,T)$ obtained at a pressure ($P$) and temperature ($T$) in each experiment and $K_D(P_0,T)$ calculated from thermodynamic parameters determined at $P_0 = 25$ GPa in this study, $\Delta V^0$ for each experimental result is calculated from

$$\Delta V^0 = RT \ln[K_D(P,T,X)/K_D(P_0,T,X)]/(P_0 - P). \quad (5)$$

The calculated $\Delta V^0$ value for each experiment is shown in Figure 6. Uncertainties are estimated by propagating the uncertainties in $K_D$ and pressure as reported in the literature. Calculated $\Delta V^0$ values are positive and almost constant from 40 to 110 GPa with an average value of $0.20 \pm 0.04$ cm$^3$/mol. Below 40 GPa, this calculation has large uncertainties due to the small deviations of pressure from $P_0 = 25$ GPa. The $\Delta V^0$ values for multianvil experiments performed to 50 GPa by *Tange et al.* [2009] are also calculated (Figure 6) and result in average volumes that are consistent with other studies, even though a very Fe-rich bulk composition was employed. Figure 6 therefore provides an effective way of comparing the effect of pressure alone on partitioning because variations in Fe content and temperature should be effectively normalized in this analysis.

[22] Using the average value of $\Delta V^0$, the enthalpy change $\Delta H^0$ for reaction (2) is further refined to be 22.3 kJ/mol. With the obtained $\Delta V^0$ and $\Delta H^0$ values, equation (3) becomes

$$RT \ln K_D = -22300 - 200P - 4.0T + 4900\left(1 - 2X_{FeSiO3}^{Pv}\right) + (11000 + 110P)\left(1 - 2X_{FeO}^{Fp}\right), \quad (6)$$

where pressure ($P$) is in GPa and temperature ($T$) is in K.

[23] Using equation (6), $K_D$ for the $(Mg_{0.9},Fe_{0.1})_2SiO_4$ composition at 2000 K is calculated up to 120 GPa (solid line in Figure 5). At 100 GPa, $K_D$ is calculated to be 0.16 with an uncertainty (shaded region in Figure 5) of $\pm$ 0.03 based on the volume change error.

[24] It should be noted that some of the discrepancies in $K_D$, measured in DAC investigations [*Auzende et al.*, 2008; *Sakai et al.* 2009; *Sinmyo et al.*, 2008], result from variations in the bulk Fe contents and temperatures of individual studies. These discrepancies appear much smaller, however, when the actual Fe contents of the phases involved are considered. The model predicts a change in the Mg-Pv Fe/(Fe + Mg) ratio for a $(Mg_{0.9},Fe_{0.1})_2SiO_4$ bulk composition from 0.048 at 25 GPa to 0.031 at 100 GPa, a relatively small shift for a large pressure change. At 100 GPa conflicting experimental Mg-Pv Fe/(Fe + Mg) ratios lie in the range 0.026–0.036, which is also very small, particularly when compared to the analytical uncertainties of at least $\pm$0.01 in this ratio as determined from results of DAC studies. Therefore, although experimental $K_D$ values seem to be quite widely scattered in Figure 5 the actual differences in Fe contents between phases at similar conditions are relatively small and calculating $K_D$ tends to exaggerate these small differences.

[25] *Auzende et al.* [2008] and *Sakai et al.* [2009] reported an abrupt reduction in $K_D$ at around 70–100 GPa and attributed this to the $Fe^{2+}$ electronic spin transition from high-spin to low-spin in Fp. As shown in Figure 6 there is no consistent shift in the determined volume change of equilibrium (2), even within results from a single study. It is therefore hard

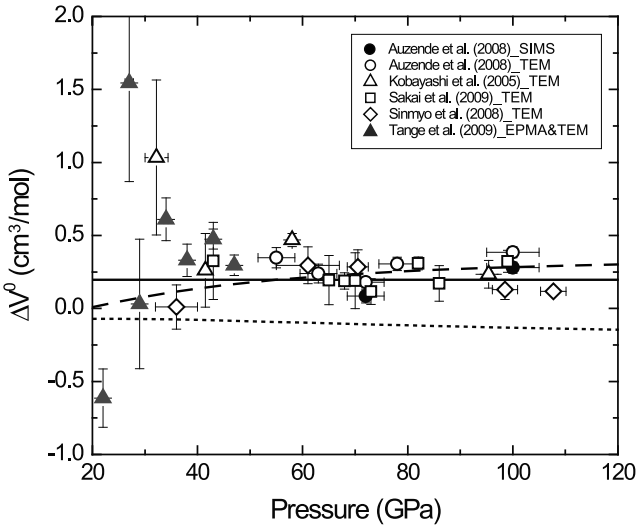


**Figure 6.** The standard state volume change for the Fe-Mg exchange reaction between perovskite and ferropericlase as a function of pressure. The volumes are estimated from individual DAC and multianvil experimental partitioning results using the thermodynamic model derived in this study at 25 GPa (see text for details). The solid line shows the average volume change of $0.20 \pm 0.02$ cm$^3$/mol obtained from a fit to the data (see text for details). The dotted line is calculated from the thermodynamic parameters given in *Xu et al.* [2008]. The dashed line is calculated from same model modified with the recent experimental results by *Tange et al.* [2009] and *Fischer et al.* [2011], as described for Figure 5.

to argue that the DAC results cannot be explained by a single value of $\Delta V^0$ or a value changing only as a response to elastic compression. In fact, it is doubtful that the spin transition in Fp can cause abrupt changes in partitioning behavior in this system. Experimental and theoretical studies show that the $Fe^{2+}$ spin state in Fp changes gradually over a broad pressure range at high temperature (e.g., over the range 50–90 GPa at 2000 K for $Mg_{0.75}Fe_{0.25}O$) [*Lin et al.*, 2007; *Tsuchiya et al.*, 2006]. Moreover, *Li* [2007] suggested from calculations based on crystal field theory that $K_D$ would not change abruptly due to the spin transition even if it did occur sharply over a narrow pressure range.

[26] There are several possible additional reasons for the scatter in the results of the DAC studies. (1) *Sinmyo et al.* [2008] reported that large heterogeneities in the compositions of Mg-Pv and Fp in recovered DAC samples are caused by large temperature gradients across the samples during laser heating. This can potentially result in erroneous partition coefficients that are simply transient as Fe diffuses in or out of each phase at different rates. (2) Fe-Mg diffusion in Mg-Pv is extremely sluggish, even at high temperatures [*Holzapfel et al.*, 2005] so that equilibration may not always be achieved. For these reasons it is crucial that DAC studies are supported by thermodynamic calculations based on measurements of properties that can be obtained independently and with smaller realistic uncertainties than DAC chemical partitioning data. Effects on $K_D$ from Fe-spin transitions are only likely to show up once such thermodynamic analyses are performed and may be too gradual to cause clearly detectable changes in $K_D$ over narrow pressure intervals.

### 4.3. $Fe^{3+}$ Concentrations in Al-Free and Al-Bearing Perovskite

[27] $K_D(app)$ (i.e., determined from analyses in which $Fe = Fe^{2+} + Fe^{3+}$) has been found to increase strongly with the Al content of Mg-Pv due to a strong coupling between Al and $Fe^{3+}$ substitution in Mg-Pv, although in detail the relationship is not linear [*Wood and Rubie*, 1996; *Frost and Langenhorst*, 2002; *McCammon et al.*, 2004]. Previous studies indicate that the presence of Al and $Fe^{3+}$ in Mg-Pv does not significantly influence $Fe^{2+}$-Mg partitioning between Mg-Pv and Fp and when the $Fe^{3+}$ content is measured and subtracted from the bulk perovskite Fe content, the actual $K_D$ is, within error, the same as that determined in the Al-free system [*Frost and Langenhorst*, 2002; *McCammon et al.*, 2004]. Therefore, if the $Fe^{2+}$ content of Mg-Pv can be estimated from the corresponding Fe content of Fp, using determinations of $K_D$, then any additional Fe found in Mg-Pv can be assigned to be $Fe^{3+}$. In this way the $Fe^{3+}$ contents of Mg-Pv can be determined from chemical analyses in the literature where no explicit measurement of the $Fe^{3+}/\Sigma Fe$ ratio has been made.

[28] Based on chemical analyses of phases from previous experimental studies, the $Fe^{2+}$ contents of Mg-Pv were calculated from the corresponding Fe contents of Fp and appropriate $K_D$ values for the *P-T* conditions of each experiment, using the thermodynamic parameters obtained in the current study. The $Fe^{3+}$ contents of Mg-Pv were then calculated as the difference between the determined $Fe^{2+}$ contents and the reported total Fe contents in Mg-Pv (Figure 7). In the calculations, $Fe^{3+}$ concentrations in Fp were assumed to be negligible for experiments performed in Fe and diamond capsules but for Re capsules a $Fe^{3+}/\Sigma Fe$ ratio of 0.1 was assumed (Figure 3). In this way Mg-Pv analyses from previous experimental studies performed at 21–30 GPa and 1573–2473 K have been evaluated. Experiments performed at temperatures <2273 K for time scales <1 h were excluded from this treatment on the grounds that chemical equilibrium is unlikely to have been achieved [*Katsura and Ito*, 1996; *Frost and Langenhorst*, 2002].

[29] The calculated $Fe^{3+}$ contents, $X_{Fe^{3+}}$ ($= Fe^{3+}/Fe^{2+} + Fe^{3+} + Mg$), of Mg-Pv coexisting with Fp synthesized in several different capsule materials are plotted as a function of the total Fe content of Mg-Pv in Figure 7. Based on the determined uncertainties of the thermodynamic parameters and their interdependencies (inset of Figure 4), the typical uncertainty of calculated $Fe^{3+}$ contents is $\pm 0.004$. Clearly defined trends are observed as a function of different capsule materials and the presence of Al in the samples. Along each trend, there is good agreement between samples where $Fe^{3+}/\Sigma Fe$ ratios have been measured and those that have been estimated using the method described above. For Al-free samples the Mg-Pv $Fe^{3+}/\Sigma Fe$ ratios calculated for samples equilibrated in rhenium capsules [*Katsura and Ito*, 1996; *Martinez et al.*, 1997; *Frost and Langenhorst*, 2002; *McCammon et al.*, 2004] are in the range 0.1–0.3, which is in good agreement with results from ELNES and Mössbauer spectroscopy measurements [*Frost and Langenhorst*, 2002; *McCammon et al.*, 2004]. Lower $Fe^{3+}/\Sigma Fe$ values are estimated for Al-free Mg-Pv samples synthesized in diamond

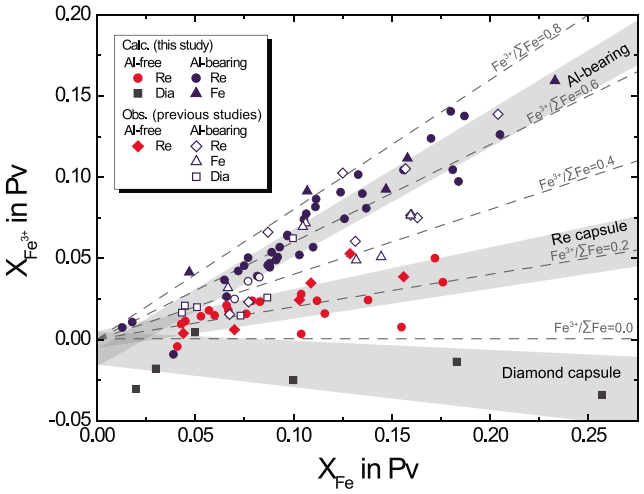


**Figure 7.** Calculated $Fe^{3+}$ contents of Mg-perovskite coexisting with ferropericlase in Al-free and Al-bearing systems. $X_{Fe^{3+}}$ (= $Fe^{3+}/Fe^{2+} + Fe^{3+} + Mg$) values are plotted as a function of $X_{Fe}$ (= $[Fe^{2+} + Fe^{3+}]/[Fe^{2+} + Fe^{3+} + Mg]$). Mg-Pv $Fe^{3+}$ concentrations were calculated from results of previous experiments performed on Al-free and Al-bearing systems using a variety of capsule materials (see text for details). Black squares and filled red circles show the results of experiments on the Al-free system using diamond [*Tange et al.*, 2009; *Yamazaki et al.*, 2009] and rhenium (Re) capsules [*Frost and Langenhorst*, 2002; *Katsura and Ito*, 1996; *Martinez et al.*, 1997], respectively. Solid blue symbols show results for Al-bearing samples contained in Re and metallic iron (Fe) capsules [*Frost and Langenhorst*, 2002; *Hirose et al.*, 2001; *Nishiyama and Yagi*, 2003; *Wood*, 2000]. Open blue symbols and red diamonds show results based on direct measurements of $Fe^{3+}$ in Pv [*Frost and Langenhorst*, 2002; *Frost et al.*, 2004; *Irifune et al.*, 2010; *McCammon et al.*, 2004]. Broken lines show ferric iron ratios $Fe^{3+}/(Fe^{2+} + Fe^{3+})$ in Mg-Pv. Shaded areas indicate uncertainties on linear fits to data obtained in different capsules and for Al-bearing samples.

capsules [*Tange et al.*, 2009; *Yamazaki et al.*, 2009] compared to those in rhenium capsules. This is in good agreement with the expected oxygen fugacity range for the different capsule types, as experiments in diamond capsules are constrained to be at least 4 orders of magnitude lower in $fo_2$ compared to the maximum $fo_2$ obtainable in Re capsules at 25 GPa and 2000 K [*Pownceby and O'Neill*, 1994; *Stagno and Frost*, 2010]. Even though the capsule material should only influence the upper $fo_2$ limit, it seems that, at least for Al-free experiments, the capsule material employed has a clear influence on the $fo_2$ and corresponding $Fe^{3+}$ concentrations. This may be the result of the capsule environment in the multianvil being intrinsically oxidizing as a result of the routine use of $LaCrO_3$ furnaces, such that all capsule materials become oxidized to some extent and metals such as Re likely form an oxide buffer. $Fe^{3+}/\Sigma Fe$ ratios that are estimated to be lower than zero in Figure 7 most likely arise due to disequilibrium as Fe-Mg equilibration between Mg-Pv and Fp is extremely sluggish at low $fo_2$ and temperatures <2200 K [*Frost and Langenhorst*, 2002].

[30] In Al-bearing systems, $Fe^{3+}/\Sigma Fe$ ratios are significantly higher than those in the Al-free system and cover a broader range of values, from 0.2 to 0.8. Figure 8 shows the relationship between $Fe^{3+}$ and Al concentrations in Mg-Pv with values calculated from previous studies using the method outlined above [*Frost and Langenhorst*, 2002; *Hirose et al.*, 2001; *Nishiyama and Yagi*, 2003; *Wood*, 2000] compared with observed values where $Fe^{3+}/\Sigma Fe$ ratios were actually measured [*Frost and Langenhorst*, 2002; *Frost et al.*, 2004; *Irifune et al.*, 2010; *Lauterbach et al.*, 2000; *Li et al.*, 2004; *Miyajima et al.*, 2004; *McCammon et al.*, 2004; *Saikia et al.*, 2009]. The agreement between measured and estimated values is good and it can be seen that there is no clear trend separating experiments performed in Re, Pt, Au, diamond or Fe capsules, which is also apparent in Figure 7.

[31] The relationship between Al and $Fe^{3+}$ in Mg-Pv has been shown to be nonlinear [*Frost and Langenhorst*, 2002], which is likely related to the changing mechanism of 3+ cation incorporation. However, in Figure 8 the data have also been contoured as a function of bulk Fe concentration and it is clear that the $Fe^{3+}$ content also depends relatively linearly on bulk Fe.

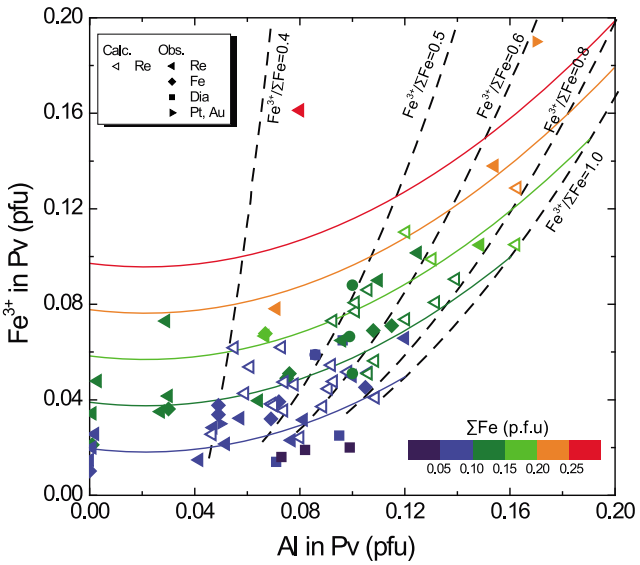


**Figure 8.** The relationship between $Fe^{3+}$ and Al concentration in Mg-perovskite in atoms per formula unit (pfu) normalized to two cations. The color variation indicates the bulk Fe content in Mg-perovskite (Mg-Pv). Open symbols show $Fe^{3+}$ contents of Mg-Pv calculated from previous studies [*Frost and Langenhorst*, 2002; *Hirose et al.*, 2001; *Nishiyama and Yagi*, 2003; *Wood*, 2000] using the present thermodynamic model (see text). Filled symbols show measurements of $Fe^{3+}$ in Mg-Pv synthesized in capsules consisting of noble metals (Re, Pt, Au), Fe metal, and diamond [*Frost and Langenhorst*, 2002; *Frost et al.*, 2004; *Irifune et al.*, 2010; *Lauterbach et al.*, 2000; *Li et al.*, 2004; *Miyajima et al.*, 2004; *McCammon et al.*, 2004; *Saikia et al.*, 2009]. Solid lines are fitted curves for different total Fe ($\Sigma Fe$ = 0.05–0.25) and Al contents with the form: $x_{Fe^{3+}} = \alpha_0 x_{Al} + \alpha_1 x_{Al}^2 + \beta_0 x_{\Sigma Fe}$. Broken lines indicate $Fe^{3+}/\Sigma Fe$ ratio contours.

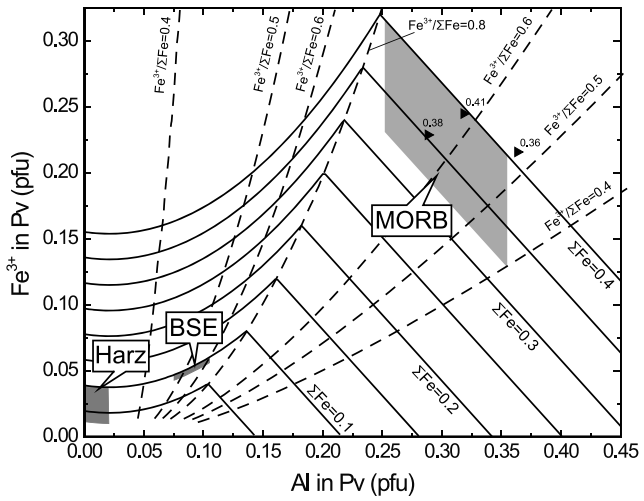


**Figure 9.** $Fe^{3+}$ and Al concentrations for ranges of plausible lower mantle Mg-perovskite compositions. Broken lines are contours of $Fe^{3+}/\Sigma Fe$ ratio and solid lines give $Fe^{3+}$ and Al concentrations for different bulk iron ($\Sigma Fe$) contents. The maximum value of $Fe^{3+}/\Sigma Fe$ is assumed to be 0.8, in line with experimental observations. The $Fe^{3+}$ contents increase with Al content up to $Fe^{3+}/\Sigma Fe = 0.8$, and decrease linearly with Al content beyond this maximum ratio, as discussed in the text. Symbols with corresponding total $\Sigma Fe$ values indicated are from measurements by *Litasov et al.* [2003]. The ranges of $Fe^{3+}$ and Al contents of Mg-Pv are indicated for peridotitic or bulk silicate Earth (BSE), harzburgitic (Harz), and basaltic (MORB) compositions by gray shaded regions based on the results of previous studies [*Hirose et al.*, 1999; *Irifune*, 1994; *Irifune and Ringwood*, 1987; *Ono et al.*, 2001].

[32] Two possible mechanisms can be considered for $Fe^{3+}$ and $Al^{3+}$ incorporation into a $Mg^{2+}Si^{4+}O_3$ perovskite structure [e.g., *McCammon*, 1998; *Frost and Langenhorst*, 2002] in which two distinct sites are the pseudo-dodecahedral A-site for 2+ cations and the octahedral B-site for $Si^{4+}$ [e.g., *Horiuchi et al.*, 1987]. One is a coupled substitution mechanism by which both the A- and B-sites are occupied by 3+ cations along the compositional join $MgSiO_3$-$Fe^{3+}Al^{3+}O_3$. In this substitution, $Fe^{3+}$ occupies the A-site and is charge balanced by $Al^{3+}$ located on the octahedral site, as determined for Al-rich Fe-bearing Mg-Pv (Al = 0.08 per formula unit, pfu) [*Miyajima et al.*, 2004]. The second is an oxygen vacancy mechanism by which 3+ cations occupy only B-sites along the join $Mg^{2+}Si^{4+}O_3$-$Mg^{2+}Fe^{3+}O_{2.5}$ (or $Mg^{2+}Al^{3+}O_{2.5}$) and charge balance is achieved by oxygen vacancy formation. The stoichiometry determined from chemical analyses of some $Al^{3+}$-poor Fe-bearing Mg-Pv is consistent with the oxygen defect mechanism [e.g., *Lauterbach et al.*, 2000; *Frost and Langenhorst*, 2002]. In Al-poor Fe-bearing Mg-Pv (Al = 0.03 pfu), Mössbauer measurements indicate that tetrahedrally coordinated $Fe^{3+}$ might be located on the normally octahedrally coordinated Si site [*Lauterbach et al.*, 2000], which would be consistent with the existence of local oxygen-vacancies. This site occupancy of $Fe^{3+}$ is also observed in perovskites in the system $CaTiO_3$-$Ca^{2+}Fe^{3+}O_{2.5}$ [e.g., *Becerro et al.*, 1999]. A strong linear relationship between Al and $Fe^{3+}$ concentrations in Mg-Pv is expected for the coupled substitution mechanism while for the oxygen vacancy mechanism the relationship would likely be weaker [*Frost and Langenhorst*, 2002].

[33] For Al contents <0.08 pfu, the $Fe^{3+}$ content varies mainly with bulk Fe and only weakly with Al. This is most likely due to the dominance of an oxygen vacancy mechanism for 3+ cation incorporation. At higher Al contents (>0.08 pfu), the relationship between Al and $Fe^{3+}$ concentrations becomes stronger and a 1:1 interdependence is approached. This results from the emerging dominance of a coupled substitution mechanism. The data in Figure 8 have been parameterized with a simple empirical relationship to describe the $Fe^{3+}$ content as a function of bulk Fe and Al:

$$x_{Fe3+} = \alpha_0 x_{Al} + \alpha_1 x_{Al}^2 + \beta_0 x_{\Sigma Fe}. \quad (7)$$

The fitted parameters are $\alpha_0 = -0.13 \pm 0.07$, $\alpha_1 = 3.1 \pm 0.5$., and $\beta_0 = 0.39 \pm 0.03$. Using this empirical relationship, both Mg-Pv $Fe^{3+}$ contents obtained by our calculations and direct measurements are reproduced within $\pm 0.012$ pfu and $\pm 0.022$ pfu for 68% and 95% confidence limits, respectively, for the 78 data points plotted in Figure 8.

[34] Although it may be possible to produce a perovskite with $Fe^{3+}/\Sigma Fe = 1$, for any given bulk Fe content a limit in Al content will be reached where insufficient $Fe^{3+}$ is available on the A-site to balance Al in the B-site. Experiments employing mid-oceanic ridge basalt (MORB) bulk compositions indicate that it is indeed possible to produce Al-rich Mg-Pv where insufficient $Fe^{3+}$ exists to balance Al in the B-site [*Litasov et al.*, 2003]. The stoichiometry of such samples, shown in Figure 9, is such that Al must start to also substitute onto the A-site, and $Fe^{3+}$ contents decrease as a result of charge balance on the B-site being now being maintained partly by Al on the A-site. This most likely occurs because at any given pressure there is a limit to the solubility of Al on the B-site, which is in accordance with experiments performed in the Fe-free system [*Irifune et al.*, 2002]. It then becomes energetically more favorable for $Fe^{3+}$ to be replaced by Al, and the dependence of Al-bearing Mg-Pv on $Fe^{3+}$ decreases. This is shown by the downward trending bulk Fe contours in Figure 9, which indicates a 1:1 inverse dependence of $Fe^{3+}$ on Al. It can be seen that the high Al and Fe Mg-Pv samples synthesized by *Litasov et al.* [2003] fit these downward trending contours very well. However, it is unclear whether or not the trend can be applied for the high Al but low Fe compositional range as no data exist for these compositions.

### 4.4. Implications for $Fe^{3+}$ Concentrations in the Lower Mantle

[35] Knowledge of the chemical composition of Mg-Pv as a function of bulk rock composition, pressure and temperature is important for most geophysical calculations of lower mantle properties. The currently prevailing view is that the lower mantle dominantly has a peridotitic or bulk silicate Earth (BSE) composition [e.g., *Irifune et al.*, 2010]. However, it must also contain chemical heterogeneities arising from the subduction of oceanic lithosphere with crustal and depleted mantle lithologies that were originally basaltic and harzburgitic. Because Al and bulk Fe contents of these

rocks are quite different, Mg-Pv that forms in these different lithologies should contain different concentrations of these two elements. In addition, the Al contents of Mg-Pv in some bulk compositions will change due to the disappearance or appearance of aluminous phases such as majoritic garnet, depending on phase stability. Using the relationship among $Fe^{3+}$, $Al^{3+}$ and bulk Fe of Mg-Pv obtained in this study, it is possible to determine the range in $Fe^{3+}$ contents for plausible lower mantle rock compositions (Figure 9).

[36] At the very top of the lower mantle, ~660 km depth, the Mg-Pv that initially forms by the breakdown of ringwoodite in a peridotitic i.e., BSE bulk composition [e.g., *McDonough and Sun*, 1995] will have a relatively low Al content of 0.02 pfu because Al will reside mainly in coexisting majoritic garnet [*Wood*, 2000], which persists within the top 30–40 km of the lower mantle. Some uncertainty exists as to whether Mg-Pv $Fe^{3+}$ contents depend on $fo_2$ at these low Al concentrations. Analyses of Al-free Mg-Pv synthesized in Fe capsules have reported $Fe^{3+}/\Sigma Fe$ ratios <0.1–0.2 [*Lauterbach et al.*, 2000]. The total Fe content of Mg-Pv at the top of the lower mantle will be approximately 0.09 pfu and the corresponding $Fe^{3+}$ content will, therefore, be of the order of 0.01–0.02. At these low Al contents it is likely that a significant proportion of the 3+ cations substituting into the Mg-Pv Si site (B-site) will have charge balance maintained by the creation of oxygen vacancies. At greater depths, however, majoritic garnet will break down and by 720 km depth the bulk of the Al in a BSE composition will partition into Mg-Pv, resulting in an Al content in the range 0.08–0.11 [*Irifune*, 1994]. For a BSE composition, Mg-Pv with this level of Al will persist throughout the lower mantle [*Irifune et al.*, 2010], resulting in an $Fe^{3+}$ content of 0.05–0.06 pfu and $Fe^{3+}/\Sigma Fe$ ratios in the range 0.5–0.6. At such concentrations it is likely that the coupled substitution of $Fe^{3+}$ and Al starts to dominate as the main substitution mechanism. Similar $Fe^{3+}/\Sigma Fe$ ratios (0.52–0.67) were measured by *Irifune et al.* [2010] for Al-bearing Mg-Pv synthesized up to pressures of 47 GPa. The bulk Fe content of Mg-Pv in a BSE composition at depths greater than 720 km should be approximately 0.10 pfu. Although *Irifune et al.* [2010] reported a drop in $K_D(app)$ for Mg-Pv and Fp formed from a BSE composition between 25 and 47 GPa, this drop corresponds to a change in bulk Fe content of Mg-Pv of only 0.02 pfu, which is relatively small and is unlikely to significantly influence mineral properties. It is, however, hard to explain this drop, which seems to result mainly from $Fe^{2+}$-Mg exchange. Over the same pressure interval the model derived in this study, from Al-free DAC results described above, would predict a drop of only 0.006 pfu.

[37] Subducted depleted lithospheric mantle with a harzburgitic bulk composition [e.g., *Michael and Bonatti*, 1985] will form Mg-Pv with a similar Al content to that formed from a BSE composition at the top of the lower mantle (<~0.02 pfu) [*Irifune and Ringwood*, 1987]. The low Al content, which is inherent to the bulk composition, will persist, however, throughout the Mg-Pv stability field. Given bulk Fe contents of 0.09 pfu for Mg-Pv in a harzburgite composition, the $Fe^{3+}$ content will lie, as described above, in the range 0.01–0.03 pfu and the oxygen vacancy substitution mechanism will likely remain dominant.

[38] A number of experiments have been performed to determine the mineralogy of a mid-oceanic ridge basalt (MORB) composition in the lower mantle. At 25–30 GPa, Mg-Pv containing Al in the range 0.25–0.35 pfu and bulk Fe between 0.32 and 0.40 pfu has been reported [*Hirose et al.*, 1999; *Litasov and Ohtani*, 2005; *Ono et al.*, 2001] with the variation mainly reflecting the particular bulk composition selected. As described at the end of the previous section, the measured $Fe^{3+}/\Sigma Fe$ ratios for such Al-rich perovskites are about 0.6 [*Litasov et al.*, 2003], with $Fe^{3+}$ contents on the order of 0.20–0.25 pfu that are insufficient to allow all Al to be charge balanced on the Si site. Some Al is therefore accommodated in the Mg-site, reducing $Fe^{3+}$ and causing the negative $Fe^{3+}$ dependence on Al shown in Figure 9. The Mg-Pv Al contents of MORB are in the range where this $AlAlO_3$ substitution starts to take over from the $Fe^{3+}AlO_3$ substitution. The situation at pressures higher than 25–30 GPa is more uncertain. Mg-Pv may be able to accommodate more Al on the Si site at higher pressures, as suggested by the study of *Nishio-Hamane et al.* [2005], who synthesized perovskite with 25% of the $Fe^{3+}AlO_3$ component at 50 GPa.

[39] Variations in rock composition in the lower mantle will, therefore, result in large variations in Mg-Pv $Fe^{3+}$ contents due to differences in Al and bulk Fe contents. These changes also reflect differences in the dominant 3+ cation substitution mechanisms, with the corresponding Mg-Pv 3+ cation components varying from $MgAlO_{2.5}$ at low Al contents to $Fe^{3+}AlO_3$ for BSE compositions and additionally $AlAlO_3$ for MORB bulk compositions. Most importantly, however, such changes in the 3+ substitution mechanism in Mg-Pv and the corresponding variations in $Fe^{3+}$ and oxygen vacancy concentrations probably result in differences in physical properties between major chemical heterogeneities in the mantle, including viscosity, electrical conductivity, thermal conductivity and elasticity.

[40] **Acknowledgments.** We thank Heinz Fischer, Stefan Übelhack, and Detlef Krauße for technical assistance and Hubert Schulze for the preparation of MgO single-crystal capsules. Florian Heidelbach and Sushant Shekhar are thanked for assistance with EBSD measurements. We are grateful to Ryosuke Sinmyo for constructive discussion and Reider Trønnes and an anonymous reviewer for their constructive comments. This project was financially supported by the Bayerisches Geoinstitut Visitor's Program for Y.N.

## References

Auzende, A.-L., J. Badro, F. J. Ryerson, P. K. Weber, S. J. Fallon, A. Addad, J. Siebert, and G. Fiquet (2008), Element partitioning between magnesium silicate perovskite and ferropericlase: New insights into bulk lower-mantle geochemistry, *Earth Planet. Sci. Lett.*, *269*, 164–174, doi:10.1016/j.epsl.2008.02.001.

Badro, J., G. Fiquet, F. Guyot, J.-P. Rueff, V. V. Struzhkin, G. Vanko, and G. Monaco (2003), Iron partitioning in Earth's mantle: Toward a deep lower mantle discontinuity, *Science*, *300*, 789–791, doi:10.1126/science.1081311.

Becerro, A. I., C. A. McCammon, F. Langenhorst, F. Seifert, and A. Angel (1999), Oxygen vacancy ordering in $CaTiO_3$-$CaFeO_{2.5}$ perovskites: From isolated defects to infinite sheets, *Phase Transit.*, *69*, 133–146, doi:10.1080/01411599908208014.

Benz, H. M., and J. E. Vidale (1993), Sharpness of upper-mantle discontinuities determined from high-frequency reflections, *Nature*, *365*, 147–150, doi:10.1038/365147a0.

Fabrichnaya, O. B., S. K. Saxena, P. Richet, and E. F. Westrum (2004), *Thermodynamic Data, Models and Phase Diagrams in Multicomponent Oxide Systems*, Springer, New York.

Fei, Y., L. Zhang, A. Corgne, H. Watson, A. Ricolleau, Y. Meng, and V. Prakapenka (2007), Spin transition and equations of state of (Mg,Fe)O

solid solutions, *Geophys. Res. Lett.*, *34*, L17307, doi:10.1029/2007GL030712.

Fischer, R., A. J. Campbell, G. A. Shofner, O. T. Lord, P. Dera, and V. B. Prakapenka (2011), Equation of state and phase diagram of FeO, *Earth Planet. Sci. Lett.*, *304*, 496–502, doi:10.1016/j.epsl.2011.02.025.

Frost, D. J. (2003), $Fe^{2+}$-Mg partitioning between garnet, magnesiowüstite, and $(Mg,Fe)_2SiO_4$ phases of the transition zone, *Am. Mineral.*, *88*, 387–397.

Frost, D. J., and F. Langenhorst (2002), The effect of $Al_2O_3$ on Fe-Mg partitioning between magnesiowüstite and magnesium silicate perovskite, *Earth Planet. Sci. Lett.*, *199*, 227–241, doi:10.1016/S0012-821X(02)00558-7.

Frost, D. J., F. Langenhorst, and P. A. van Aken (2001), Fe-Mg partitioning between ringwoodite and magnesiowüstite and the effect of pressure, temperature and oxygen fugacity, *Phys. Chem. Miner.*, *28*, 455–470, doi:10.1007/s002690100181.

Frost, D. J., C. Liebske, F. Langenhorst, C. A. McCammon, R. G. Trønnes, and D. C. Rubie (2004), Experimental evidence for the existence of iron rich metal in the Earth's lower mantle, *Nature*, *428*, 409–412, doi:10.1038/nature02413.

Hirose, K. (2002), Phase transitions in pyrolitic mantle around 670-km depth: Implications for upwelling of plumes from the lower mantle, *J. Geophys. Res.*, *107*(B4), 2078, doi:10.1029/2001JB000597.

Hirose, K., Y. Fei, Y. Ma, and H. Mao (1999), The fate of subducted basaltic crust in the Earth's lower mantle, *Nature*, *397*, 53–56, doi:10.1038/16225.

Hirose, K., Y. Fei, S. Ono, Y. Yagi, and K. Funakoshi (2001), In situ measurements of the phase transition boundary in $Mg_3Al_2Si_3O_{12}$: Implications for the nature of the seismic discontinuities in the Earth's mantle, *Earth Planet. Sci. Lett.*, *184*, 567–573, doi:10.1016/S0012-821X(00)00354-X.

Holland, T. J. B., and R. Powell (2011), An improved and extended internally consistent thermodynamic dataset for phases of petrological interest, involving a new equation of state for solids, *J. Metamorph. Geol.*, *29*, 333–383, doi:10.1111/j.1525-1314.2010.00923.x.

Holzapfel, C., D. C. Rubie, D. J. Frost, and F. Langenhorst (2005), Fe-Mg interdiffusion in $(Mg,Fe)SiO_3$ perovskite and lower mantle reequilibration, *Science*, *309*, 1707–1710, doi:10.1126/science.1111895.

Horiuchi, H., E. Ito, and D. J. Weidner (1987), Perovskite-type MgSiO3: Single-crystal X-ray diffraction study, *Am. Mineral.*, *72*, 357–360.

Irifune, T. (1994), Absence of an aluminous phase in the upper part of the Earth's lower mantle, *Nature*, *370*, 131–133, doi:10.1038/370131a0.

Irifune, T., and A. E. Ringwood (1987), Phase transformations in a harzburgite composition to 26 GPa: Implications for dynamical behaviour of the subducting slab, *Earth Planet. Sci. Lett.*, *86*, 365–376, doi:10.1016/0012-821X(87)90233-0.

Irifune, T., H. Naka, T. Sanehira, T. Inoue, and K. Funakoshi (2002), In situ X-ray observations of phase transitions in $MgAl_2O_4$ spinel to 40 GPa using multianvil apparatus with sintered diamond anvils, *Phys. Chem. Miner.*, *29*, 645–654, doi:10.1007/s00269-002-0275-1.

Irifune, T., T. Shinmei, C. A. McCammon, M. Miyajima, D. C. Rubie, and D. J. Frost (2010), Iron partitioning and density changes of pyrolite in Earth's lower mantle, *Science*, *327*, 193–195, doi:10.1126/science.1181443.

Ito, E., and E. Takahashi (1989), Postspinel transformations in the system $Mg_2SiO_4$-$Fe_2SiO_4$ and some geophysical implications, *J. Geophys. Res.*, *94*, 10,637–10,646, doi:10.1029/JB094iB08p10637.

Katsura, T., and E. Ito (1996), Determination of Fe-Mg partitioning between perovskite and magnesiowüstite, *Geophys. Res. Lett.*, *23*, 2005–2008, doi:10.1029/96GL02086.

Katsura, T., and S. Kimura (1965), Equilibria in the system FeO-Fe2O3-MgO at 1,160°C, *Bull. Chem. Soc. Jpn.*, *38*, 1664–1670, doi:10.1246/bcsj.38.1664.

Kobayashi, Y., T. Kondo, E. Ohtani, N. Hirao, N. Miyajima, T. Yagi, T. Nagase, and T. Kikegawa (2005), Fe-Mg partitioning between (Mg,Fe)SiO3 post-perovskite, perovskite, and magnesiowüstite in the Earth's lower mantle, *Geophys. Res. Lett.*, *32*, L19301, doi:10.1029/2005GL023257.

Lauterbach, S., C. A. McCammon, P. van Aken, F. Langenhorst, and F. Seifert (2000), Mössbauer and ELNES spectroscopy of (Mg,Fe)(Si, Al)$O_3$ perovskite: A highly oxidized component of the lower mantle, *Contrib. Mineral. Petrol.*, *138*, 17–26, doi:10.1007/PL00007658.

Li, J. (2007), Electronic transitions and spin states in perovskite and post-perovskite, in *Post-Perovskite: The Last Mantle Phase Transition*, *Geophys. Monogr. Ser.*, vol. 174, edited by K. Hirose et al., pp. 47–68, AGU, Washington, D. C., doi:10.1029/174GM06.

Li, J., V. V. Struzhkin, H.-K. Mao, J. Shu, R. J. Hemley, Y. Fei, B. Mysen, P. Dera, V. Prakapenka, and G. Shen (2004), Electronic spin state of iron in lower mantle perovskite, *Proc. Natl. Acad. Sci. U. S. A.*, *101*, 14,027–14,030, doi:10.1073/pnas.0405804101.

Lin, J. F., V. V. Struzhkin, S. D. Jacobsen, M. Y. Hu, P. Chaw, J. Kung, H. Liu, H.-K. Mao, and R. J. Hemley (2005), Spin transition of iron in magnesiowüstite in Earth's lower mantle, *Nature*, *436*, 377–380, doi:10.1038/nature03825.

Lin, J. F., G. Vanko, S. D. Jacobsen, V. Iota, V. V. Struzhkin, V. B. Prakapenta, A. Kuznetsov, and C.-S. Yoo (2007), Spin transition zone in Earth's lower mantle, *Science*, *317*, 1740–1743, doi:10.1126/science.1144997.

Litasov, K. D., and E. Ohtani (2005), Phase relations in hydrous MORB at 18–28 GPa: Implications for heterogeneity of the lower mantle, *Phys. Earth Planet. Inter.*, *150*, 239–263, doi:10.1016/j.pepi.2004.10.010.

Litasov, K., E. Ohtani, F. Langenhorst, H. Yurimoto, T. Kubo, and T. Kondo (2003), Water solubility in Mg-perovskites and water storage capacity in the lower mantle, *Earth Planet. Sci. Lett.*, *211*, 189–203, doi:10.1016/S0012-821X(03)00200-0.

Mann, U., D. J. Frost, and D. C. Rubie (2009), Evidence for high-pressure core–mantle differentiation from the metal–silicate partitioning of lithophile and weakly siderophile elements, *Geochim. Cosmochim. Acta*, *73*, 7360–7386, doi:10.1016/j.gca.2009.08.006.

Mao, H. K., G. Shen, and R. J. Hemley (1997), Multivariable dependence of Fe-Mg partitioning in the lower mantle, *Science*, *278*, 2098–2100, doi:10.1126/science.278.5346.2098.

Martinez, I., Y. Wang, F. Guyot, R. C. Liebermann, and J. C. Doukhan (1997), Microstructures and iron partitioning in (Mg,Fe)SiO3 perovskite-(Mg,Fe)O magnesiowüstite assemblages: An analytical transmission electron microscopy study, *J. Geophys. Res.*, *102*, 5265–5280, doi:10.1029/96JB03188.

McCammon, C. A. (1992), Magnetic properties of $Fe_xO$ (x > 0.95): Variation of Néel temperature, *J. Magn. Magn. Mater.*, *104–107*, 1937–1938, doi:10.1016/0304-8853(92)91612-W.

McCammon, C. A. (1998), The crystal chemistry of ferric iron in $Fe_{0.05}Mg_{0.95}SiO_3$ perovskite as determined by Mössbauer spectroscopy in the temperature range 80–293 K, *Phys. Chem. Miner.*, *25*, 292–300, doi:10.1007/s002690050117.

McCammon, C. A., M. Hutchison, and J. Harris (1997), Ferric iron content of mineral inclusions in diamonds from Sao Luiz: A view into the lower mantle, *Science*, *278*, 434–436, doi:10.1126/science.278.5337.434.

McCammon, C. A., S. Lauterbach, F. Seifert, F. Langenhorst, and P. A. van Aken (2004), Iron oxidation state in lower mantle mineral assemblages I. Empirical relations derived from high-pressure experiments, *Earth Planet. Sci. Lett.*, *222*, 435–449, doi:10.1016/j.epsl.2004.03.018.

McDonough, W. F., and S. Sun (1995), The composition of the Earth, *Chem. Geol.*, *120*, 223–253, doi:10.1016/0009-2541(94)00140-4.

Michael, P., and E. Bonatti (1985), Peridotite composition from the North Atlantic: Regional and tectonic variations and implications for partial melting, *Earth Planet. Sci. Lett.*, *73*, 91–104, doi:10.1016/0012-821X(85)90037-8.

Miyajima, N., F. Langenhorst, D. J. Frost, and T. Yagi (2004), Electron channeling spectroscopy of iron in majoritic garnet and silicate perovskite using a transmission electron microscope, *Phys. Earth Planet. Inter.*, *143–144*, 601–609, doi:10.1016/j.pepi.2003.07.023.

Nishio-Hamane, D., T. Nagai, K. Fujino, Y. Seto, and N. Takafuji (2005), $Fe^{3+}$ and Al solubilities in $MgSiO_3$ perovskite: Implication of the $Fe^{3+}AlO_3$ substitution in $MgSiO_3$ perovskite at the lower mantle condition, *Geophys. Res. Lett.*, *32*, L16306, doi:10.1029/2005GL023529.

Nishiyama, N., and T. Yagi (2003), Phase relation and mineral chemistry in pyrolite to 2200°C under the lower mantle pressures and implications for dynamics of mantle plumes, *J. Geophys. Res.*, *108*(B5), 2255, doi:10.1029/2002JB002216.

O'Neill, H. S. C., M. Pownceby, and C. A. McCammon (2003), The magnesiowüstite: Iron equilibrium and its implications for the activity–composition relations of $(Mg,Fe)_2SiO_4$ olivine solid solutions, *Contrib. Mineral. Petrol.*, *146*, 308–325, doi:10.1007/s00410-003-0496-4.

Ono, S., E. Ito, and T. Katsura (2001), Mineralogy of subducted basaltic crust (MORB) from 25 to 37 GPa, and chemical heterogeneity of the lower mantle, *Earth Planet. Sci. Lett.*, *190*, 57–63, doi:10.1016/S0012-821X(01)00375-2.

Pownceby, M. I., and H. S. C. O'Neill (1994), Thermodynamic data from redox reactions at high temperatures: IV. Calibration of the Re-$ReO_2$ oxygen buffer from EMF and NiO + Ni-Pd sensor measurements, *Contrib. Mineral. Petrol.*, *118*, 130–137, doi:10.1007/BF01052864.

Saikia, A., T. Boffa-Ballaran, and D. J. Frost (2009), The effect of Fe and Al substitution on the compressibility of MgSiO3-perovskite determined through single-crystal X-ray diffraction, *Phys. Earth Planet. Inter.*, *173*, 153–161, doi:10.1016/j.pepi.2008.11.006.

Sakai, T., E. Ohtani, H. Terasaki, N. Sawada, Y. Kobayashi, M. Miyahara, M. Nishijima, N. Hirao, Y. Ohishi, and T. Kikegawa (2009), Fe-Mg partitioning between perovskite and ferropericlase, *Am. Mineral.*, *94*, 921–925, doi:10.2138/am.2009.3123.

Sinmyo, R., K. Hirose, D. Nishio-Hamane, Y. Seto, K. Fujino, N. Sata, and Y. Ohishi (2008), Partitioning of iron between perovskite/postperovskite

and ferropericlase in the lower mantle, *J. Geophys. Res.*, *113*, B11204, doi:10.1029/2008JB005730.

Srečec, I., A. Ender, E. Woermann, W. Gans, E. Jacobsson, G. Eriksson, and E. Rosen (1987), Activity-composition relations of the magnesiowüstite solid solution series in equilibrium with metallic iron in the temperature range 1,050–1,400 K, *Phys. Chem. Miner.*, *14*, 492–498, doi:10.1007/BF00308284.

Stacey, F. D., and P. M. Davis (2004), High pressure equations of state with applications to the lower mantle and core, *Phys. Earth Planet. Inter.*, *142*, 137–184, doi:10.1016/j.pepi.2004.02.003.

Stagno, V., and D. J. Frost (2010), Carbon speciation in the asthenosphere: Experimental measurements of the redox conditions at which carbonate-bearing melts coexist with graphite or diamond in peridotite assemblages, *Earth Planet. Sci. Lett.*, *300*, 72–84, doi:10.1016/j.epsl.2010.09.038.

Stixrude, L., and C. Lithgow-Bertelloni (2011), Thermodynamics of mantle minerals–II. Phase equilibria, *Geophys. J. Int.*, *184*, 1180–1213, doi:10.1111/j.1365-246X.2010.04890.x.

Tange, Y., E. Takahashi, Y. Nishihara, K. Funakoshi, and N. Sata (2009), Phase relations in the system MgO-FeO-$SiO_2$ to 50 GPa and 2000°C: An application of experimental techniques using multianvil apparatus with sintered diamond anvils, *J. Geophys. Res.*, *114*, B02214, doi:10.1029/2008JB005891.

Tsuchiya, T., R. M. Wentzcovitch, C. R. S. da Silva, and S. de Gironcoli (2006), Spin transition in magnesiowüstite in Earth's lower mantle, *Phys. Rev. Lett.*, *96*, 198501, doi:10.1103/PhysRevLett.96.198501.

Wood, B. J. (2000), Phase transformations and partitioning relations in peridotite under lower mantle conditions, *Earth Planet. Sci. Lett.*, *174*, 341–354, doi:10.1016/S0012-821X(99)00273-3.

Wood, B. J., and D. C. Rubie (1996), The effect of alumina on phase transformations at the 660-km discontinuity from Fe-Mg partitioning experiments, *Science*, *273*, 1522–1524, doi:10.1126/science.273.5281.1522.

Xu, W., C. Lithgow-Bertelloni, L. Stixrude, and J. Ritsema (2008), The effect of bulk composition and temperature on mantle seismic structure, *Earth Planet. Sci. Lett.*, *275*, 70–79, doi:10.1016/j.epsl.2008.08.012.

Yamazaki, D., T. Yoshino, T. Matsuzaki, T. Katsura, and A. Yoneda (2009), Texture of (Mg,Fe)$SiO_3$ perovskite and ferro-periclase aggregate: Implications for rheology of the lower mantle, *Phys. Earth Planet. Inter.*, *174*, 138–144, doi:10.1016/j.pepi.2008.11.002.